energies

MDPI

Article

Two-Stage Chance-Constrained Coordinated Operation of an Integrated Gas–Electric System

Yuqi Zhang, Chuan He *, Anqi Xv and Xiaoxiao Tang

College of Electrical Engineering, Sichuan University, Chengdu 610065, China; zhang_yuqi@stu.scu.edu.cn (Y.Z.); anqi_xv@outlook.com (A.X.); txxxdrtl2003107@stu.scu.edu.cn (X.T.)
* Correspondence: he_chuan@scu.edu.cn

Abstract: Under the background that the high penetration of renewable energy generation, which mainly consists of wind power, will have a significant impact on electric power systems due to the volatility and uncertainty of renewable energy, energy systems with gas–electric coupling and interconnections have been widely studied to accommodate renewable energy generation. This paper proposes a two-stage chance-constrained coordinated operation model of an integrated gas–electric system and fully considers the uncertainty and high penetration of wind power. The Taylor series expansion method is used to linearize the Weymouth gas flow equation of a natural gas system and finally obtains a mixed integer linear programming model. Case studies show the effectiveness of the integrated energy system for peak shaving, valley filling, and promoting wind power accommodation. The proposed model ensures the consumption of wind power generation and also reduces the operation cost by about 0.7%.

Keywords: integrated gas–electric systems; chance constraint; two-stage; Taylor series expansion; penetration; MILP

Citation: Zhang, Y.; He, C.; Xv, A.; Tang, X. Two-Stage Chance-Constrained Coordinated Operation of an Integrated Gas–Electric System. *Energies* **2022**, *15*, 4458. https://doi.org/10.3390/en15124458

Academic Editor: Konstantin Suslov

Received: 22 May 2022
Accepted: 13 June 2022
Published: 18 June 2022

1. Introduction

As environmental pollution and the energy crisis have attracted worldwide attention, renewable energy is gradually replacing traditional fossil fuel energy. Among all the renewable energy sources, on-shore wind energy accounted for 25.1% in 2021 [1], indicating that on-shore wind energy is significant in the energy market. The renewable energy represented by wind energy plays a vital role in an electrical power system (EPS). However, wind power generation is volatile and wind spillage frequently occurs. This is an issue that requires an urgent solution [2,3]. How to promote the consumption of renewable energy has become one of the critical issues widely considered by the academic community. The integrated energy system represented by the integrated gas–electric system (IGES) provides a solution to the problem of renewable energy adoption [4]. The gas–electric system uses power-to-gas (P2G) equipment to convert electric energy into the chemical energy of natural gas fuel and uses gas-fired units to convert the chemical energy of natural gas fuel into electricity to achieve a two-way energy flow between the EPS and the natural gas system. The combination of P2G equipment and energy storage systems (ESSs) can improve wind power spillage to an extent. With the increasing penetration of wind power generation in EPSs, the traditional dispatching model cannot ensure the security of the power system operation [5]. Therefore, it is of significance to propose a reasonable and solvable optimal scheduling model for an IGES with the presence of the penetration of renewable energy generation and an ESS.

Many scholars have undertaken research on the comprehensive optimization of integrated gas–electric systems, including the influence and operational function of P2G equipment on an IGES and the formulation and linearization method of an IGES model [6]. Clegg and Mancarella introduced an original methodology to analyze different P2G processes and assess their operational impacts on both electricity networks and gas networks,

carried out by using a novel integrated model specifically developed for the simulation of the operational interdependencies between the two networks and considering P2G equipment [7]. Zlotnik et al. applied new techniques for the control of dynamic gas flows on pipeline networks to examine the day-ahead scheduling of electric generator dispatch and gas compressor operation for different levels of integration, spanning from separate forecasting and simulation to a combined optimal control [8]. Considering the high interdependency between gas and electricity networks, Ref. [9] proposed an interval optimization model that included demand response, uncertain wind power generation, and the nonlinear characteristics of a pipeline gas flow. Alvarez proposed a two-stage stochastic model that integrated electric power with hydraulic and natural gas systems and considered several effects; a mixed integer linear programming (MILP) model and a reduction algorithm to reduce the computational burden of the scenarios were implemented [10]. Li et al. proposed a security-constrained bi-level economic dispatch model for integrated natural gas and electricity systems considering wind power and power-to-gas (P2G); the bi-level optimization model was transformed into a MILP formulation for a solution [11].

The high penetration of renewable energy generation and the uncertainty model of renewable energy are taken into account in an IGES model. Xue et al. analyzed the impact of uncertain wind power generation on the system security, power quality, economic efficiency, and social welfare of an EPS [12]. Qiu et al. [13] used chance constraints to ensure that the wind energy utilized met a minimal level at a certain probability and developed a deterministic approximation approach using sample average approximation (SAA) and provided a strong extended formulation. Duan et al. established a distributed coordinated optimization model of integrated electricity–gas distribution networks considering P2G equipment and gas-fired units to solve the uncertainty problems of wind power generation [14]. Liang et al. proposed a novel adaptive optimization method that optimized the value of the uncertainty budget to minimize the size of the uncertainty set whilst considering the underlying risk of wind generation fluctuations residing outside the proposed uncertainty set [15]. Almasabi et al. proposed a cost–benefit analysis for measuring the benefits of integrating wind farms into the power grid whilst considering the dynamic operations and security of the system [16]. Shahidehpour et al. examined the impact of renewable sources of energy such as pumped storage units and photovoltaic/battery systems on power system security by reducing the dependence of the electricity infrastructure on the natural gas infrastructure [17]. Zeng et al. proposed an iterative method to solve the nonlinearity in the model and studied the impact of power and natural gas systems on the daily economic dispatch [18].

With the wide use of ESSs in EPSs, which plays an important role in improving the quality of renewable energy generation, the impact of ESSs on IGESs is a nonignorable factor. Many scholars have conducted research on the modeling of ESSs coordinated with the uncertainty of wind power in IGESs. Zhang et al. proposed a market-oriented optimal scheduling strategy that included a wind farm with a multi-stage hybrid ESS and analyzed the function of the ESS in different phases of the electrical market [19]. Liu et al. constructed a wind power supply chain with ESS participation and explored benefit coordination on the basis of the dual effort cost. The paper established a noncooperative pricing model and a cooperative pricing model and proposed four benefit distribution strategies based on different influencing factors. It was found that, considering the impact of the dual effort cost, cooperative pricing was more conducive to the consumption of wind power and an improvement in the overall benefits of the wind power supply chain [20]. Dadashi et al. presented a novel strategy of multiple wind producers coordinated with a battery energy storage system (BESS) in the form of a strategic virtual power plant (VPP) and proposed a bi-level programming framework in which the expected profit of the VPP was maximized at the upper level through solving a two-stage stochastic problem. The paper also conducted a sensitivity analysis to investigate the effect of the BESS on the optimal operation and expected benefits of the wind-based VPP [21]. Luo et al. established a mathematical model of wind power and an ESS for a simulation and analysis; the results

showed that the wind power prediction was reasonable as the power quality and stability of the wind farm connected to the power grid could be improved by the ESS [22]. Li et al. proposed a novel day-ahead scheduling model for a district IGES in the presence of severe uncertainty caused by a high penetration of wind power and employed an information gap decision theory to better depict the inherent uncertainty of wind power considering compressed air energy storage and a demand response program to reduce the system operation costs as well as the impact of wind power uncertainty [23]. de Boer et al. focused on the economic and environmental system consequences from the application of P2G and pumped hydro storage and compressed air energy storage into an electricity system at different wind power penetration levels [24].

Aiming at the optimal operation of an IGES with a high penetration of wind power generation and an ESS, in this paper we propose a chance-constrained coordinated scheduling model of an IGES considering the uncertainty of wind generation. In this model, the chance-constrained method is used to describe the uncertainty of wind power. The Taylor series expansion (TSE) method is utilized to linearize the nonlinear Weymouth equation, which converts the nonlinear optimization problem into a mixed integer linear programming (MILP) problem.

The major contributions of the paper are twofold:

(1) In this paper, we propose a two-stage chance-constrained coordinated scheduling model of an IGES considering the uncertainty of wind power generation. The first stage minimizes the operation cost according to a base-case scenario and the second stage ensures that a certain range of wind generation is accommodated via chance constraints.

(2) Chance constraints describing the utilization of wind power are recast into a group of mixed integer linear constraints via a strong extended formulation for a sample average approximation. In addition, nonlinear Weymouth equations are linearized by the Taylor series expansion method, where pressure recovery is further carried out to obtain high quality solutions.

2. Deterministic Scheduling Model

2.1. Objective Function

In order to minimize the total operation cost of the IGES, the objective function was indicated as per Equation (1); the operation cost of the gas-fired units was included in the production cost of the natural gas well.

$$\min \sum_t \left\{ \sum_{i \in NGU} C_i^{fuel} \cdot [F_i^c(P_{it}) + SU_{it} + SD_{it}] + \sum_j C_j^G \cdot G_{jt} + \sum_s C_s^E \cdot E_{st} \right\} \quad (1)$$

where NGU represents the set of thermal power units; i is the index of the generating units; t is the index of the time; s is the index of the ESS; j is the index of the natural gas well; P_{it} represents the output of the thermal power unit, i; $F_i^c(P_{it})$ is the coal fuel consumption of unit i when its power generation equals P_{it}; SU_{it} and SD_{it} are the startup and shutdown fuel costs, respectively, of unit i; C_i^{fuel} is the fuel price of unit i; C_j^G is the production cost of the natural gas well, j; G_{jt} is the production of the natural gas well, j; C_s^E is the operation cost of the ESS s; and E_{st} is the energy storage volume of the ESS, s.

2.2. Constraints of an EPS

The normal operation of an EPS satisfies the constraints of nodal power balance (Equation (2)). The constraints of the energy flow in the transmission line, which is described in the DC power flow method, are shown in Equation (3), the constraints of the maximum and minimum limits of the transmission lines are shown in Equation (4), the constraints of the bus angle are shown in Equation (5), the constraints of the power generation limit are shown in Equation (6), the ramping constraints of the thermal power units

and gas-fired units are shown in Equations (7)–(10), and the constraints of the start-up and shutdown times are shown in Equations (11) and (12).

$$\sum_{i\in N(e)} P_{it} + \sum_{w\in N(e)} P_{wt} + \sum_{s\in N(e)} P_{st} + \sum_{r(l)\in N(e)} PL_{lt} - \sum_{s(l)\in N(e)} PL_{lt} = \sum_{d\in N(e)} P_{dt} \quad (2)$$

$$PL_{lt} = \left(\theta_{s(l)t} - \theta_{r(l)t}\right)/x_l \quad (3)$$

$$-PL_l^{max} \le PL_{lt} \le PL_l^{max} \quad (4)$$

$$\theta_e^{min} \le \theta_{et} \le \theta_e^{max} \quad (5)$$

$$P_i^{min}\cdot I_{it} \le P_{it} \le P_i^{max}\cdot I_{it} \quad (6)$$

$$P_{it} - P_{i(t-1)} \le UR_i\cdot I_{i(t-1)} + P_i^{min}\cdot\left(I_{it} - I_{i(t-1)}\right) + P_i^{max}\cdot(1 - I_{it}) \quad (7)$$

$$P_{i(t-1)} - P_{it} \le DR_i\cdot I_{it} + P_i^{min}\cdot\left(I_{i(t-1)} - I_{it}\right) + P_i^{max}\cdot\left(1 - I_{i(t-1)}\right) \quad (8)$$

$$SU_{it} \ge su_i\cdot\left(I_{it} - I_{i(t-1)}\right),\ SU_{it} \ge 0 \quad (9)$$

$$SD_{it} \ge sd_i\cdot\left(I_{i(t-1)} - I_{it}\right),\ SD_{it} \ge 0 \quad (10)$$

$$\left(X_{i(t-1)}^{on} - T_i^{on}\right)\cdot\left(I_{i(t-1)} - I_{it}\right) \ge 0 \quad (11)$$

$$\left(X_{i(t-1)}^{off} - T_i^{off}\right)\cdot\left(I_{it} - I_{i(t-1)}\right) \ge 0 \quad (12)$$

The wind power generation at each time period was limited by the predicted wind power generation (Equation (13)) and its total utilization was constrained by Equation (14) to ensure a certain consumption level.

$$0 \le P_{wt} \le P_{f,wt} \quad (13)$$

$$\sum_w\sum_t P_{wt} \ge \alpha\cdot\sum_w\sum_t P_{f,wt} \quad (14)$$

where $P_{f,wt}$ is the predicted wind power output of the wind power unit, w, and α is the percent of the wind power utilization.

The constraints of energy storage included the balance of storage capacity (Equation (15)), the maximum and minimum limits of charge and discharge (Equations (16) and (17)), and the characteristic of the energy storage, which was that the ESS should not be discharging and charging at the same time (Equation (18)).

$$E_{st} = E_{s(t-1)} + \eta_s^{CHA}\cdot P_{st}^{CHA} - \frac{P_{st}^{DIS}}{\eta_s^{DIS}} \quad (15)$$

$$I_{st}^{CHA}\cdot P_{st}^{CHA,min} \le P_{st}^{CHA} \le I_{st}^{CHA}\cdot P_{st}^{CHA,max} \quad (16)$$

$$I_{st}^{DIS}\cdot P_{st}^{DIS,min} \le P_{st}^{DIS} \le I_{st}^{DIS}\cdot P_{st}^{DIS,max} \quad (17)$$

$$P_{st} = P_{st}^{DIS} - P_{st}^{CHA} \quad (18)$$

$$I_{st}^{CHA} + I_{st}^{DIS} \le 1 \quad (19)$$

2.3. Constraints of a Natural Gas System

A gas system is an energy system that mainly consists of gas-fired units, a gas pipeline, P2G equipment, a compressor, a gas well, and a gas load that has similar characteristics to an EPS. A gas turbine is a type of internal combustion engine that continuously converts chemical energy generated by gas fuel into mechanical and electric energy. A gas turbine unit model is presented in Equations (20) and (21). P2G equipment can effectively convert

excess renewable energy generation into natural gas to decrease renewable energy spillage. P2G equipment is capable of providing assistance for the EPS, such as load balancing, the efficient consumption of renewable energy power generation, and auxiliary services. Its model can be presented as per Equations (22) and (23).

$$G_{it} = \frac{F(P_{it}) + SU_{it} + SD_{it}}{HHV}, \ \ i \in GU \tag{20}$$

$$F(P_{it}) = a_i \cdot (P_{it})^2 + b_i \cdot P_{it} + c_i, \ \ i \in GU \tag{21}$$

$$G_{at} = (\phi \cdot P_{at} \cdot \eta_a)/HHV \tag{22}$$

$$0 \le P_{at} \le P_a^{max} \cdot I_{at} \tag{23}$$

The operational constraints of a natural gas system consist of node power balance constraints (Equation (24)), natural gas flow constraints that can be expressed as nonlinear Weymouth equations (Equations (25)–(27)), the gas production constraints of natural gas wells (Equation (28)), and the constraints of the compressors that maintain the pressure of the gas system (Equation (29)).

$$\begin{gathered}\sum_{j \in G(m)} G_{jt} + \sum_{r(mn) \in G(m)} G_{mn,t} - \sum_{s(mn) \in G(m)} G_{mn,t} + \sum_{r(c) \in G(m)} GL_{c,t} - \\ \sum_{s(c) \in G(m)} GL_{c,t} + \sum_{a \in G(m)} G_{at} = \sum_{g \in G(m)} G_{gt} + \sum_{i \in G(m)} G_{it}\end{gathered} \tag{24}$$

$$G_{mn,t} = \mathrm{sgn}(\pi_{mt}, \pi_{nt}) \cdot K_{mn} \cdot \sqrt{|\pi_{mt}^2 - \pi_{nt}^2|} \tag{25}$$

$$\mathrm{sgn}(\pi_{mt}, \pi_{nt}) = \begin{cases} 1, \ \pi_{mt} \ge \pi_{nt} \\ -1, \ \pi_{mt} < \pi_{nt} \end{cases} \tag{26}$$

$$\pi_m^{min} \le \pi_{mt} \le \pi_m^{max} \tag{27}$$

$$G_j^{min} \le G_{jt} \le G_j^{max} \tag{28}$$

$$\pi_{nt} \le \Gamma_c \cdot \pi_{mt} \tag{29}$$

2.4. Abstract Formulation

The above deterministic scheduling model can be written in a general abstract form as Equations (30)–(32). Equation (31) represents the constraints associated with the binary variables only whereas Equation (32) represents all operational constraints.

$$\min \boldsymbol{ax} + \boldsymbol{by} \tag{30}$$

$$s.t. \boldsymbol{Ax} \le \boldsymbol{C} \tag{31}$$

$$\boldsymbol{g}(\boldsymbol{x}, \boldsymbol{y}) \le \boldsymbol{D} \tag{32}$$

3. The Proposed Two-Stage Coordinated Operation Model

Due to the volatility and uncertainty of the output of renewable energy, introducing uncertain variables to establish chance constraints satisfies a certain confidence interval and ensures that the absorption ratio of the wind power reaches a certain level.

Considering the chance constraints of wind power generation, the deterministic scheduling model in Equations (30)–(32) can be extended to Equations (33)–(35).

$$\min \boldsymbol{ax} + \boldsymbol{by} \tag{33}$$

$$s.t. \boldsymbol{Ax} \le \boldsymbol{C} \tag{34}$$

$$Pr\{\boldsymbol{g}(\boldsymbol{x}, \boldsymbol{y}) \le \boldsymbol{D}\} > 1 - \varepsilon \tag{35}$$

Based on the above abstract model, we proposed a two-stage coordinated operation model for an IGES, which is presented as Equations (36)–(40). The first stage considered the deterministic IGES model with P2G equipment, the ESS, and deterministic wind power generation (Equations (37) and (38)). The second stage considered uncertain wind power generation with the chance constraints (Equation (39)). These two stages were coupled by a corrective ramp constraint of units (Equation (40)).

$$\min \boldsymbol{ax} + \boldsymbol{by} \tag{36}$$

$$s.t. \boldsymbol{f}(\boldsymbol{x}) \leq \boldsymbol{C} \tag{37}$$

$$\boldsymbol{g}(\boldsymbol{x}, \boldsymbol{y}) \leq \boldsymbol{D} \tag{38}$$

$$Pr\{\boldsymbol{g}(\boldsymbol{x}, \boldsymbol{y^u}) \leq \boldsymbol{D}\} > 1 - \varepsilon \tag{39}$$

$$|\boldsymbol{y} - \boldsymbol{y^u}| \leq \boldsymbol{v} \tag{40}$$

4. Solution Methodology

4.1. Reformulation of the Chance Constraint

Specifically, we transformed Equations (13) and (14) into a chance constraint (Equation (41)) [25].

$$Pr\left\{ \begin{array}{c} 0 \leq P_{wt} \leq P_{f,wt} \\ \sum_w \sum_t P_{wt} \geq \alpha \cdot \sum_w \sum_t P_{f,wt} \end{array} \right\} \geq 1 - \varepsilon \tag{41}$$

Considering the chance constraints to describe the uncertainty of wind generation, the sample average approximation (SAA) method was used to transform the chance constraints as per Equations (42)–(44).

$$\sum_w \sum_t P_{wt} + v_\varsigma \cdot M \geq \alpha \cdot \sum_w \sum_t P_{f,wt,\varsigma}, \forall \varsigma \tag{42}$$

$$P_{wt} - v_\varsigma \cdot M \leq \alpha \cdot P_{f,wt,\varsigma} \forall w, t, \varsigma \tag{43}$$

$$\sum_\varsigma v_\varsigma \leq \varepsilon |\delta| \tag{44}$$

With the conventional SAA method discussed above, the size of the constraint formulation rapidly grew as the scenario number of the chance constraint increased [26]. Therefore, we converted Equations (42)–(44) to Equations (45)–(48).

$$\sum_w \sum_t P_{wt} + v_\varsigma \cdot \left(\alpha \cdot \sum_w \sum_t P_{f,wt,\varsigma} \right) \geq \alpha \cdot \sum_w \sum_t P_{f,wt,\varsigma}, \forall \varsigma \tag{45}$$

$$\beta_{wt} + v_\varsigma \cdot \left(P_w^{max} - P_{f,wt,\varsigma} \right) \leq P_w^{max} - P_{f,wt,\varsigma}, \forall w, t, \varsigma \tag{46}$$

$$\beta_{wt} = P_w^{max} - P_{wt} \tag{47}$$

$$\sum_\varsigma v_\varsigma \leq \varepsilon |\delta| \tag{48}$$

Constraint (42) was converted to Equations (43) and (45) was converted to Equations (46) and (47). Taking Equation (42) as an example, there were two conditions: when $v_\varsigma = 0$, $\sum_w \sum_t P_{wt} \geq \alpha \cdot \sum_w \sum_t P_{f,wt,\varsigma}, \forall \varsigma$ held; when $v_\varsigma = 1$, $\sum_w \sum_t P_{wt} + v_\varsigma \cdot M \geq \alpha \cdot \sum_w \sum_t P_{f,wt,\varsigma}, \forall \varsigma$ held. Equation (45), which was converted from Equation (42), also had two conditions: when $v_\varsigma = 0$, $\sum_w \sum_t P_{wt} \geq \alpha \cdot \sum_w \sum_t P_{f,wt,\varsigma}, \forall \varsigma$ held; when $v_\varsigma = 1$, $\sum_w \sum_t P_{wt} + \alpha \cdot \sum_w \sum_t P_{f,wt,\varsigma} \geq \alpha \cdot \sum_w \sum_t P_{f,wt,\varsigma}, \forall \varsigma$ held because $P_{wt} \geq 0$. Therefore, the examples of Equations (42) and (45) indicated that Equation (45) was sufficient for Equation (42). The same analyzing method also indicated that Equations (46) and (47) were sufficient for Equation (43).

To improve the computational efficiency of these constraints, a strong extended formulation of the SAA method was employed (Equations (49)–(55)) [26]. For Equations (45)–(47), the star inequalities were used to build a strong extended formulation. We sorted $\alpha \cdot \sum_w \sum_t P_{f,wt,\varsigma}$ and

$P_w^{max} - P_{f,wt,\varsigma}$ into a descending order to study whether the wind power output satisfied the chance constraint. The strong extended formulation of the SAA method reduced the number of calculations and improved the calculation speed.

$$\alpha \cdot \sum_k \left(r_k \cdot \sum_w \sum_t P_{f,wt,\varsigma(k)} - r_k \cdot \sum_w \sum_t P_{f,wt,\varsigma(k+1)} \right) + \sum_w \sum_t P_{wt} \geq \alpha \cdot \sum_w \sum_t P_{f,wt,\varsigma(1)} \quad (49)$$

$$r_k - r_{k+1} \geq 0, \forall k \quad (50)$$

$$v_{\varsigma(k)} - r_k \geq 0, \forall k \quad (51)$$

$$\sum_k \left(\left(P_{f,wt,\varsigma(k+1)} - P_{f,wt,\varsigma(k)} \right) \cdot \gamma_{wt,k} \right) + P_w^{max} - P_{wt} \geq P_w^{max} - P_{f,wt,\varsigma(k)}, \forall w, t \quad (52)$$

$$\gamma_{wt,k} - \gamma_{wt,k+1} \geq 0, \forall k, w, t \quad (53)$$

$$v_{\varsigma(k)} - \gamma_{wt,k} \geq 0, \forall k, w, t \quad (54)$$

$$\sum_{\varsigma} v_{\varsigma} \leq \varepsilon |\delta| \quad (55)$$

4.2. Linearization of the Weymouth Equation via Taylor Series Expansion (TSE)

The nonlinear Weymouth equation is widely used in natural gas systems and caused significant difficulties in solving the model. The Taylor series expansion (TSE) method was used to linearize the Weymouth equation, transforming the nonlinear programming problem into a linear programming problem, reducing the difficulties in solving the model and improving the solution speed. Using a first-order TSE, the Weymouth equation was expressed as a linearized equation near to any fixed pressure node $\left(\pi_{mt}^0, \pi_{nt}^0\right)$ at the ends of the natural gas pipeline (Equation (56)).

$$G_{mn,t} = G_{mn,t}^0 + \frac{\partial G_{mn,t}}{\partial \pi_{mt}} \cdot \left(\pi_{mt} - \pi_{mt}^0 \right) + \frac{\partial G_{mn,t}}{\partial \pi_{nt}} \cdot \left(\pi_{nt} - \pi_{nt}^0 \right) + \Delta G_{mn,t} \quad (56)$$

where $G_{mn,t}^0$ is the transmission gas flow of the natural gas pipeline between the system nodes m and n under node pressure $\left(\pi_{mt}^0, \pi_{nt}^0\right)$; $\Delta G_{mn,t}$ is the gas flow remainder after the first-order TSE.

When we calculated the node pressure $(\hat{\pi}_{mt}, \hat{\pi}_{nt})$, we could define the number of breakpoints of the natural gas pressure as B and define the pressure of the nodes within the given range $\left(\pi_m^{min}, \pi_m^{max}\right)$ to approach the outside of the cone, presented as Equations (57)–(61).

$$G_{mn,t} \leq K_{mn} \cdot \mathrm{sgn}(\pi_{mt}, \pi_{nt}) \cdot \sqrt{\hat{\pi}_{mt}^2 - \hat{\pi}_{nt}^2} + \frac{\partial G_{mn,t}}{\partial \pi_{mt}} \cdot (\pi_{mt} - \hat{\pi}_{mt}) + \frac{\partial G_{mn,t}}{\partial \pi_{nt}} \cdot (\pi_{nt} - \hat{\pi}_{nt}) \quad (57)$$

$$G_{mn,t} \leq K_{mn} \cdot \mathrm{sgn}(\pi_{mt}, \pi_{nt}) \cdot \hat{\varphi}_{mn,t}^b \cdot \pi_{mt} - K_{mn} \cdot \mathrm{sgn}(\pi_{mt}, \pi_{nt}) \cdot \hat{\phi}_{mn,t}^b \cdot \pi_{nt} \quad (58)$$

$$\begin{cases} \hat{\pi}_{mt}^b \geq \hat{\pi}_{nt}^b \\ \pi_{mt} \geq \pi_{nt} \end{cases} \quad (59)$$

$$\hat{\varphi}_{mn,t}^b = \frac{\hat{\pi}_{mt}}{\sqrt{\left(\hat{\pi}_{mt}^b\right)^2 - \left(\hat{\pi}_{nt}^b\right)^2}} \quad (60)$$

$$\hat{\phi}_{mn,t}^b = \frac{\hat{\pi}_{nt}}{\sqrt{\left(\hat{\pi}_{mt}^b\right)^2 - \left(\hat{\pi}_{nt}^b\right)^2}} \quad (61)$$

The Weymouth natural gas power flow function was expanded by the TSE method and approximated by a series of linearized inequalities. This approximation could cause calculation errors and even obtain infeasible solutions. Therefore, we improved the objec-

tive as Equation (62) and improved the linearized Weymouth function of Equation (57) to Equation (63), which enhanced the accuracy of the TSE method [27].

$$\min \sum_t \left\{ \rho \cdot \sum_{(m,n)\in\Omega_P} \left(\xi^+_{mn,t} + \xi^-_{mn,t} \right) \right\} \tag{62}$$

$$\left(G^*_{mn,t}\right)^2 = K^2_{mn} \cdot \mathrm{sgn}(\pi_{mt}, \pi_{nt}) \cdot \left(\pi^2_{m,t} - \pi^2_{n,t} \right) + \xi^+_{mn,t} - \xi^-_{mn,t} \tag{63}$$

5. Case Studies

5.1. System Settings

In this study, a gas–electric system with a 6-bus power grid and a 7-node natural gas network was used as an example to validate the effectiveness of the proposed model. The system topology is illustrated in Figure 1; the day-ahead forecasted curves of the wind power generation, power load, and natural gas load are illustrated in Figure 2.

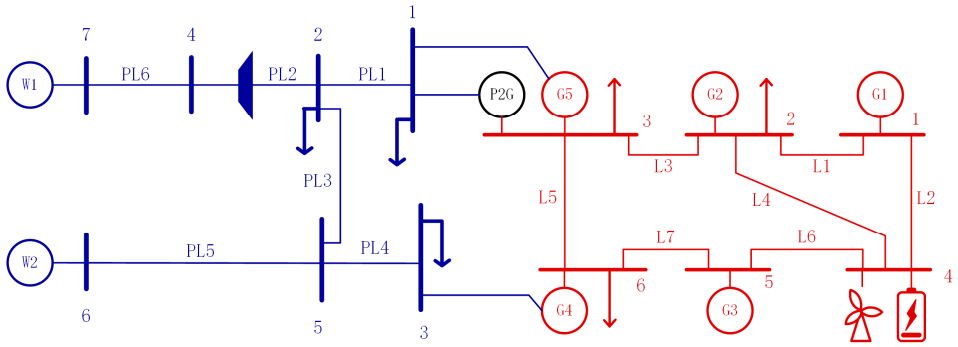

Figure 1. Topology of a 7-node NG grid with a 6-bus power grid.

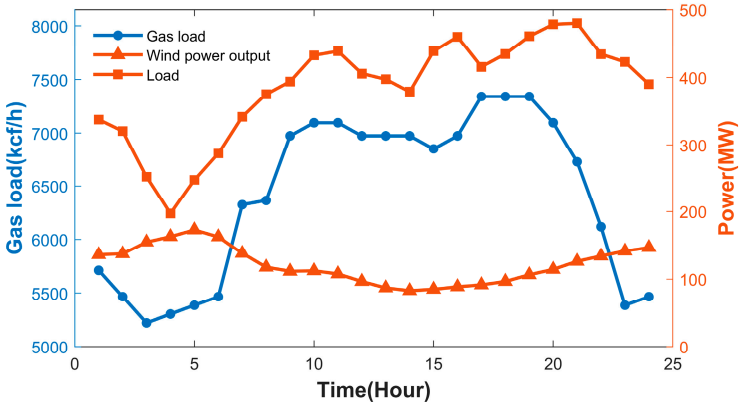

Figure 2. Forecasted wind power generation, power load, and natural gas load curve.

The 6-bus power grid consisted of 5 generating units and 7 transmission lines. Units G1, G2, and G3 represented traditional coal-fired thermal power units. The cost coefficient of the coal-fired units was 2.5 USD/MBtu. Units G4 and G5 represented the gas-fired units connected to nodes 3 and 1 of the natural gas network and bus 6 and bus 3 of the power system, respectively. The power load was at bus 2, bus 3, and bus 6 in the power grid. A wind farm with an ESS was connected to bus 4 of the power grid. The gas wells W2 and W1 were connected to nodes 6 and 7 of the natural gas network and the cost coefficients were 2 USD/kcf and 2.2 USD/kcf. The natural gas load was at nodes 1, 2, and 3. The compressor station was between nodes 2 and 4. The P2G equipment was connected to node 1 of the natural gas network and bus 3 of the power grid. The maximum conversion power of the P2G equipment was 100 MW and the conversion efficiency was 0.64. All the operation

costs of the gas units were calculated in the production cost of the natural gas well and the P2G equipment. Detailed information is presented in Tables 1 and 2.

Table 1. Parameters of generators.

Generators	G1	G2	G3	G4	G5
Lower limits (MW)	130	50	30	25	10
Upper limits (MW)	250	200	80	100	50
Ramp rates (MW/h)	125	100	40	50	40
Minimum start–stop time (h)	8	8	4	5	3
Start–stop heat consumption (MBtu)	1500	1500	100	50	50
Fuel price (USD/MBtu)	2.5	2.5	2.5	3	3

Table 2. Parameters of ESS.

Lower Limits (MW)	Upper Limits (MW)	Capacity (MW)	Efficiency
0	30	150	0.9

In the natural gas network, the Weymouth equation—which describes natural gas flow constraints—were approximated by the Taylor series expansion (TSE) method via a series of linearized inequalities. This TSE method can cause calculation errors. If the node pressure obtained by the solution was inconsistent with any given breakpoint pressure, the original Weymouth equation could not be strictly satisfied. If the node pressure obtained from the solution was closer to a given breakpoint pressure, the result was more accurate. The results in Table 3 indicate that increasing the number of breakpoints effectively improved the accuracy of the linearization approximation and sacrificed part of the calculation speed. As the inequalities processed by the Taylor series expansion method were transformed into linear constraints, a continuous increase in the number of breakpoints did not significantly increase the calculation time.

Table 3. Comparison of the accuracy of TSE method with different breakpoint numbers.

Number of Breakpoints	Maximum Relative Error	Computing Time (s)
10	1.0997×10^{-4}	0.024
45	4.3993×10^{-7}	0.032
100	1.1055×10^{-8}	0.034
500	2.1646×10^{-9}	0.034
1000	1.0550×10^{-9}	0.036

The following five cases were carried out to demonstrate the effectiveness of the proposed model.

Case 1: Deterministic model without P2G.

Case 2: Deterministic model with P2G.

Case 3: Case 2 considering basic chance constraints.

Case 4: Case 2 considering a two-stage coordinated operation with chance constraints.

Case 5: Influence of a change of coefficients in Case 4.

5.2. Deterministic Model

The results of Case 1 are presented in Table 4 The system total operation cost was USD 527,990, which consisted of USD 175,106 in coal costs and USD 352,884 in natural gas costs. The day-ahead system dispatch is illustrated in Figure 3, in which wind spillage was obviously observed at 4:00 a.m. The commitment status of the power units are shown in Figure 3 and these indicated that units G1 and G2 remained in a start-up state and unit G3 remained shut down all day; the total unit time equaled 75.

Table 4. System cost in different cases.

	Total Cost (USD)	Coal Cost (USD)	Gas Cost (USD)
Case 1	527,990	175,106	352,884
Case 2	527,838	175,106	352,732
Case 3	533,881	181,102	352,779
Case 4	530,029	178,841	351,188

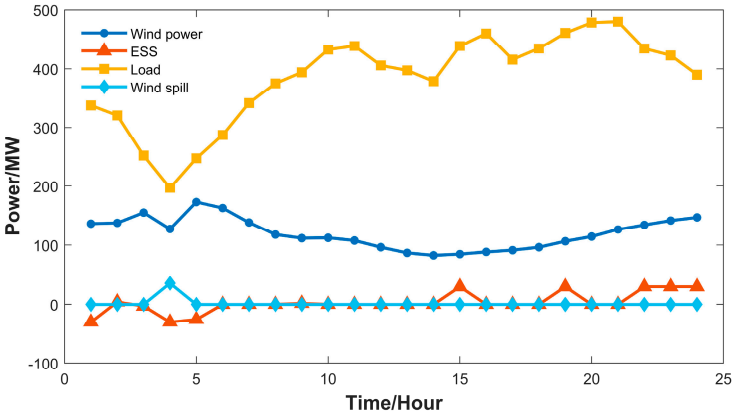

Figure 3. System operation result in Case 1.

The results of Case 2 are presented in Table 4, illustrating that as P2G could convert electricity into natural gas, the operation cost and wind spillage were lower than Case 1. The total operation cost of Case 2 was USD 527,838, which consisted of USD 175,106 of coal costs, which was the same as Case 1, and USD 352,732 of natural gas costs, which was lower than Case 1, indicating the decrease in operation costs achieved by better wind power consumption and lower wind power spillage. Compared with Case 1, due to the operation characteristics of P2G, no wind spillage occurred at 4:00 a.m., which is illustrated in Figure 4. The commitment status of the power units were same as Case 1, which are illustrated in Figure 5.

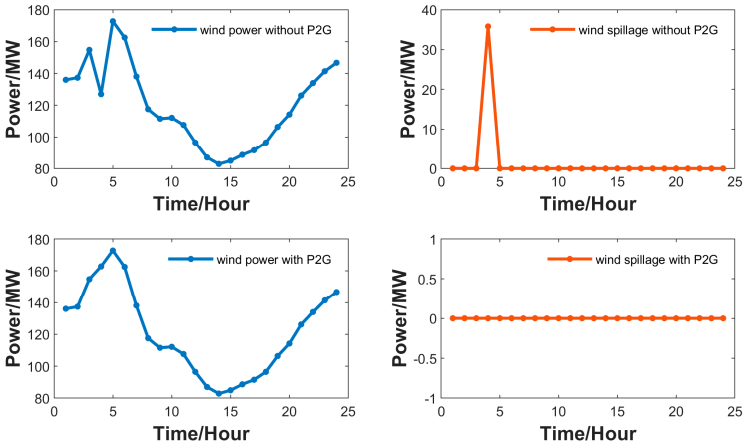

Figure 4. Wind power output and wind spillage in Case 1 and Case 2.

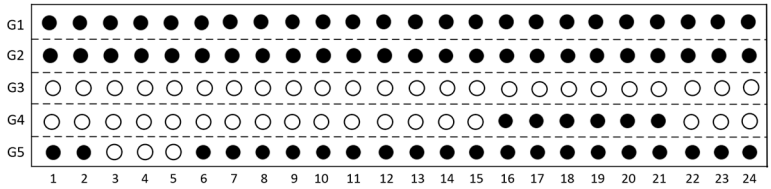

Figure 5. Commitment status of units in Case 1, Case 2, and Case 3.

5.3. Scheduling Model Considering Chance Constraints

In Case 3, considering the uncertainty of wind power generation, Equations (13) and (14) were directly transformed into chance constraints (Equations (49)–(55)). The results of Case 3 are presented in Table 4. This indicated that, when considering uncertainty, the operation costs would increase. As uncertainty fluctuations caused more wind spillage and as the utilization of wind power decreased, the fuel cost increased. The commitment status of the power units in Case 3 were the same as Case 1 and Case 2, as illustrated in Figure 5.

In Case 3, ε and α were two important parameters that noticeably affected the objective and system operation. Figure 6 indicates the objective changes with different values of ε and α. Increasing ε and α led to a lower objective and the influence of α was more subtle compared with the influence of ε. Changing α changed the percentage of wind power utilization; when the percentage was higher, other units led to a lower power generation, which consumed less fuel and resulted in a lower total operation cost. Changing ε changed the risk level of the chance constraints; when risk parameter ε was higher, the number of unacceptable scenarios increased and the total system operation cost was lower.

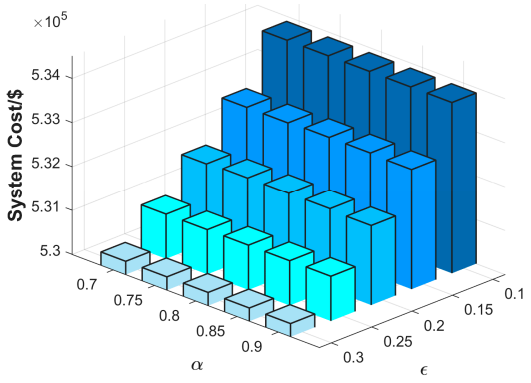

Figure 6. Objectives with different values of ε and α.

In Case 3, the scenario number and forecast error percent of wind power generation were also two important parameters that noticeably affected the objective and system operation. Figure 7 indicates the objective changes when different values of the scenario number were implemented and the forecast error percentage was changed, showing that changing the two parameters led to a lower objective. When the scenario number was larger, the uncertainty characteristics were more obvious, which led to a higher operation cost. Figure 8 shows that as the scenario number grew, the operation cost increased. When the wind forecast percentage increased, the uncertainty characteristics were more obvious, which led to a higher system operation cost.

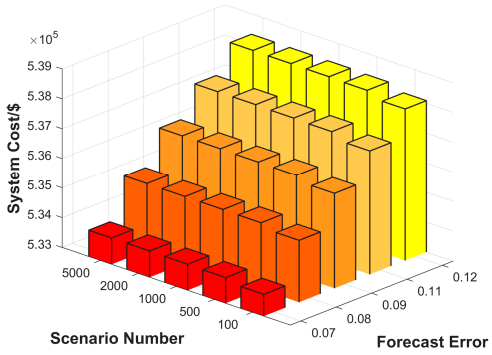

Figure 7. Objectives with different values of scenario number and wind power forecast errors.

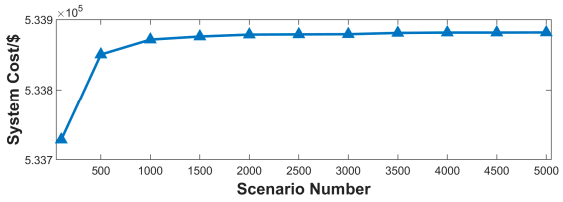

Figure 8. Objectives with different values of scenario number.

In Case 4, we applied the proposed two-stage coordinated operation model (Equations (36)–(40)). The results of Case 4 are presented in Table 4, and indicated that the operation cost was lower than that of Case 3. The commitment status of the generating units in Case 4 are illustrated in Figure 9. The commitment status of units G1, G2, G3, and G5 remained the same; unit G4 additionally started up at 15:00 p.m. and 22:00 p.m. compared with Case 3. The reason why the commitment status of unit G4 changed was that when considering the two-stage model, the fluctuation range of the wind power was limited by the ramp constraint. In other words, the deviation between the actual output and the predicted output did not exceed a certain range; therefore, to satisfy the flow balance, unit G4 had more unit time.

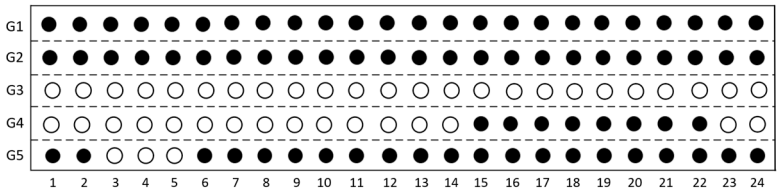

Figure 9. Commitment status of unit day-ahead in Case 4.

5.4. Sensitivity Analysis

A sensitivity analysis was carried out to study how uncertainty parameter changes affected the performance of the proposed model. In this study, we chose four factors mentioned before (ε, α, scenario number, and forecast error percent of wind power generation) as the uncertainty parameters considering different penetrations of wind generation.

This sensitivity analysis measured the unit time and system cost with changing wind power penetration when the other parameters were the same as Case 3. The results are illustrated in Figures 10 and 11. As shown in Figure 10, as penetration level increased, the unit time first decreased and then increased. Figure 11 shows that the system operation cost monotonically decreased.

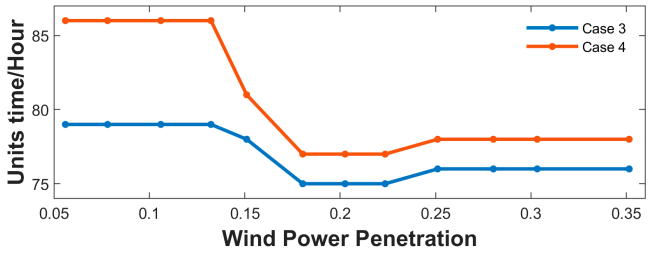

Figure 10. Unit times with different wind power penetration.

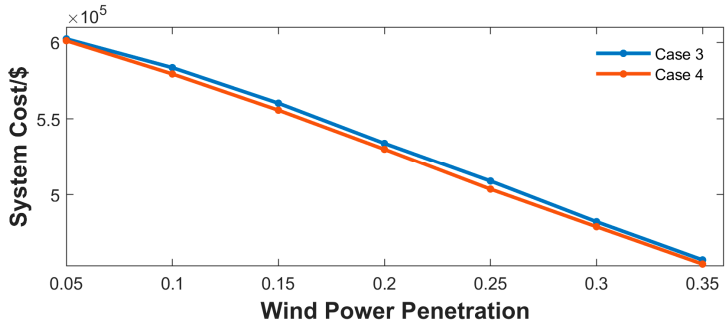

Figure 11. System cost with different wind power penetration.

The commitment status of the units are presented in Figures 12 and 13, when the penetration of the wind power generation was equal to 10% and 30%, respectively. In the penetration level equal to 10%, the unit time was 79. Compared with 20% penetration, units G1, G2, G3, and G4 had the same status during the day and unit G5 had more committed hours because of less wind power generation. With 30% penetration, the unit time equaled 76; when compared with 20% penetration, units G1, G2, and G5 had the same status during the day and units G3 and G4 had a different status at certain times to cater for the higher wind power generation and fluctuation.

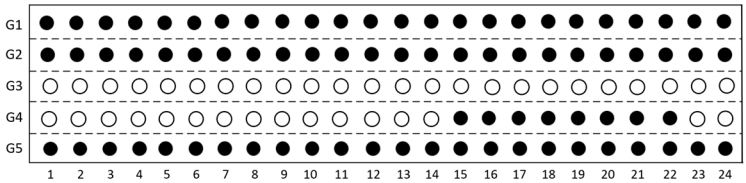

Figure 12. Commitment status of units with 10% penetration of wind power generation.

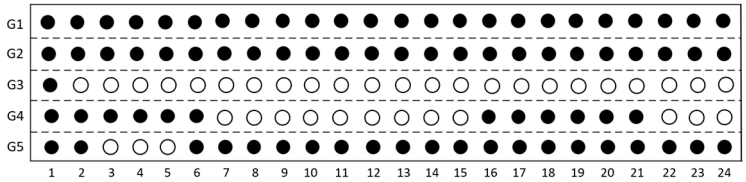

Figure 13. Commitment status of units with 30% penetration of wind power generation.

Changing the trends to 10% and 30% penetration with different uncertain model parameters had similar results to 20% penetration. All of these results indicated that when ε increased, the system cost was lower. The influence of changing α was difficult to observe. When the forecast error of wind power increased, the system cost was higher. When the scenario number increased, the system cost increased. We also observed that when penetration grew and other coefficients remained unchanged, the system cost significantly decreased. Compared with 20% penetration, 10% and 30% penetration were less sensitive with uncertainty input changes. As 10% and 30% penetration had a similar trend to 20% and were less sensitive, we discussed 20% in more detail.

Table 5 presents the results when penetration equaled 20%; ς is the scenario number and e is the forecast error of wind power. All instances that had the same unit time (e.g., instances 1–3, instances 4–6, and instances 7–8) had the same commitment status of units, as illustrated in Figure 14. Compared with Case 3, the unit time of the instances increased due to parameter changes, which led to a higher system operation cost.

Table 5. System cost in different cases.

	Parameters	Unit Time (Hours)	System Cost (USD)
Instance 1	$\alpha = 0.75, \varepsilon = 0.2, \varsigma = 5000, e = 0.0675$	75	531,832
Instance 2	$\alpha = 0.8, \varepsilon = 0.15, \varsigma = 5000, e = 0.0675$	75	532,751
Instance 3	$\alpha = 0.8, \varepsilon = 0.1, \varsigma = 2000, e = 0.1068$	75	537,411
Instance 4	$\alpha = 0.7, \varepsilon = 0.1, \varsigma = 1000, e = 0.2481$	78	550,293
Instance 5	$\alpha = 0.7, \varepsilon = 0.1, \varsigma = 2000, e = 0.2435$	78	549,882
Instance 6	$\alpha = 0.6, \varepsilon = 0.1, \varsigma = 2000, e = 0.2435$	78	549,890
Instance 7	$\alpha = 0.6, \varepsilon = 0.1, \varsigma = 1000, e = 0.3996$	79	564,679
Instance 8	$\alpha = 0.6, \varepsilon = 0.1, \varsigma = 5000, e = 0.3967$	79	564,478

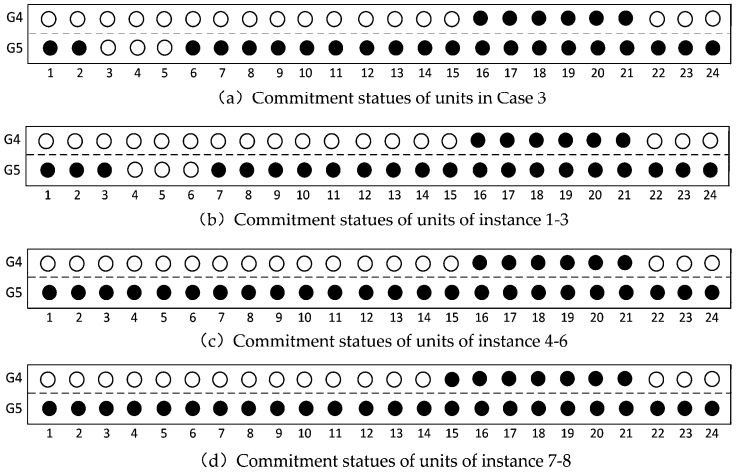

Figure 14. Commitment status of units.

6. Conclusions

In this paper, we proposed a two-stage chance-constrained coordinated operation of an IGES with an ESS and considered the uncertainty of wind generation. We analyzed the influence of P2G equipment and the ESS on the IGES operation and wind spillage as well as the impact of the nonignorable factors of chance constraints on the system cost and the influence of wind generation penetration on the system cost and commitment status of the generating units. To linearize the proposed model, which consisted of a nonlinear Weymouth equation, we used the Taylor series expansion method and obtained a solvable MILP model.

Our case studies showed the effectiveness of the ESS and integrated energy system for peak shaving, valley filling, and promoting wind power consumption. A comparison of the deterministic model with and without P2G equipment indicated that P2G equipment had ability to decrease wind spillage, leading to a lower system operation cost. It was also demonstrated that the proposed two-stage chance-constrained coordinated model had a better economy and wind accommodation. A sensitive analysis showed that 20% penetration of wind power was more sensitive than 10% and 30% penetration.

Author Contributions: Data curation, A.X.; Formal analysis, X.T.; Funding acquisition, C.H.; Investigation, Y.Z. and X.T.; Methodology, Y.Z.; Software, Y.Z.; Supervision, C.H.; Validation, A.X.;

Writing—original draft, Y.Z.; Writing—review & editing, C.H. All authors have read and agreed to the published version of the manuscript.

Funding: This work was supported in part by the Science and Technology Project of Sichuan Province 2021YFSY0051.

Data Availability Statement: Data available on request from the authors.

Conflicts of Interest: The authors declare no conflict of interest.

Nomenclature

Indices:

a	Index of P2G equipment.
c	Index of natural gas compressor.
d	Index of load.
e	Index of bus.
g	Index of natural gas load.
i	Index of generating units.
j	Index of natural gas well.
k	Index of scenarios.
l	Index of transmission line.
m, n	Index of natural gas network nodes.
s	Index of ESS.
t	Index of the time.
w	Index of wind power units.
ς	Index of scenarios.
$\varsigma(k)$	Element index in descending order.

Variables:

B	Number of breakpoints of natural gas pressure.
DR_i	Ramp-down limit of unit i.
E_{st}	Energy storage volume of ESS s.
$F_i^c(P_{it})$	Coal fuel consumption of unit i when its power generation equals P_{it}.
G_{at}	Natural gas production of P2G equipment a.
G_{gt}	Total demand of natural gas load.
G_{it}	Natural gas consumption of gas turbine unit i.
G_{jt}	Production of natural gas well j.
$G_{mn,t}$	Natural gas flow in natural gas pipeline between node m and node n.
$G_{mn,t}^0$	Transmission gas flow of natural gas pipeline between system node m and n under node pressure $\left(\pi_{mt}^0, \pi_{nt}^0\right)$.
$\Delta G_{mn,t}$	Gas flow remainder after first-order TSE.
$G_{mn,t}^*$	Natural gas flow in pipeline mn.
$GL_{c,t}$	Natural gas flow where the compressor station is located.
$G(m)$	Collection of equipment connected to node m in natural gas system.
I_{at}	Commitment status of P2G equipment a.
I_{it}	Commitment status of unit i.
I_{st}^{CHA}	Charge status of ESS s.
I_{st}^{DIS}	Discharge status of ESS s.
P_{at}	Power output of P2G equipment a.
P_{dt}	Total demand of load d.
$P_{f,wt}$	Predicted wind power output of wind power unit w.
$P_{f,wt,\varsigma}$	Predicted wind power output of scenario ς.
$P_{f,wt,\varsigma(k)}$	Predicted wind power output of scenario $\varsigma(k)$.
P_{it}	Output of thermal power unit i.
P_{st}	Output of ESS s.
P_{st}^{CHA}	Charging power of ESS s.
P_{st}^{DIS}	Discharging power of ESS s.
P_{wt}	Output of wind power unit w.
PL_{lt}	Power flow of power transmission line l.
r_k	Binary variables.

$r(c)$	Receiving node of compressor c.
$r(l)$	Receiving bus of transmission line l.
$r(mn)$	Receiving node of gas pipeline mn.
sd_i	Shutdown costs of unit i.
SD_{it}	Shutdown fuel costs of unit i.
su_i	Startup costs of unit i.
$s(c)$	Sending node of compressor c.
$s(l)$	Sending bus of transmission line l.
$s(mn)$	Sending node of gas pipeline mn.
SU_{it}	Startup fuel costs of unit i.
T_i^{off}	Minimum shutdown time of unit i.
T_i^{on}	Minimum start-up time of unit i.
UR_i	Ramp-up limit of unit i.
v_ς	Binary variable of scenario ς.
x_l	Reactance of transmission line l.
X_{it}^{off}	Shutdown time of unit i.
X_{it}^{on}	Start-up time of unit i.
α	Percent of wind power utilization.
β_{wt}	Intermediate variable represents difference between P_{wt} and P_w^{max}.
$\gamma_{wt,k}$	Binary variables.
δ	Total number of scenarios.
ε	Risk level of chance constraint.
$\varepsilon\lvert\delta\rvert$	Number of unacceptable scenarios.
θ_{et}	Phase angle of bus e.
$\theta_{r(l)t}$	Phase angles of the receiving bus of the transmission line l.
$\theta_{s(l)t}$	Phase angles of the sending bus of the transmission line l.
$\xi_{mn,t}^+, \xi_{mn,t}^-$	Auxiliary variables that help make the problem solvable.
π_{mt}, π_{nt}	Gas pressure of natural gas system node m and n.
π_{mt}^0, π_{nt}^0	Fixed pressure node.
$\hat{\pi}_{mt}, \hat{\pi}_{nt}$	Known node pressure.
$\hat{\pi}_{mt}^b$	Breakpoint node pressure in $\left(\pi_m^{min}, \pi_m^{max}\right)$.
ρ	Positive penalty factor.
Γ_c	Compression constant leading natural gas flow from low-pressure node to high-pressure node of gas network, $\Gamma_c > 1$.
Constants:	
a_i	Cost coefficient of gas turbine unit i.
b_i	Cost coefficient of gas turbine unit i.
c_i	Cost coefficient of gas turbine unit i.
C_s^E	Operation cost of ESS s.
C_i^{fuel}	Fuel price of unit i.
C_j^G	Production cost of natural gas well j.
G_j^{max}	Maximum capacity of gas well j.
G_j^{min}	Minimum capacity of gas well j.
HHV	Heating value of natural gas, which is 1.026 MBtu/kcf.
K_{mn}	Weymouth characteristic parameter of natural gas system node m and n.
M	A large enough number.
η_a	Energy convert efficiency of P2G equipment a.
η_s^{CHA}	Charge efficiency of ESS s.
η_s^{DIS}	Discharge efficiency of ESS s.
ϕ	Energy conversion coefficient, $\phi = 3.4$MBtu/MWh.
$(\cdot)^{\min/\max}$	Minimum/maximum value of a quantity.
Vectors:	
$\boldsymbol{A}, \boldsymbol{C}, \boldsymbol{D}, \boldsymbol{a}, \boldsymbol{b}$	Abstract matrices and vectors associated with coefficients of costs and constraints.
$\boldsymbol{g}(\boldsymbol{x}, \boldsymbol{y})$	Nonlinear function of binary vector $\boldsymbol{x}$ and continuous vector $\boldsymbol{y}$.
$\boldsymbol{v}$	Corrective ramp of units.
$\boldsymbol{x}$	Binary vector.
$\boldsymbol{y}$	Continuous vector.
$\boldsymbol{y^u}$	Uncertain system dispatch vectors under uncertain circumstances.

Sets and functions:

$F(\cdot)$	Heat rate curve function of gas-fired units.
GU	Set of gas-fired units.
NGU	Set of thermal power units.
$N(e)$	Set of devices connected to bus e.
$Pr\{\cdot\}$	Probability.
$\mathrm{sgn}(\pi_{mt}, \pi_{nt})$	Function of natural gas flow direction.

References

1. IRENA. Renewable Energy Technologies. 2021. Available online: https://www.irena.org/Statistics/View-Data-by-Topic/Capacity-and-Generation/Technologies (accessed on 27 April 2022).
2. Wu, C.; Zhang, X.-P.; Sterling, M. Wind power generation variations and aggregations. *CSEE J. Power Energy Syst.* **2022**, *8*, 17–38.
3. Han, D.; Ma, J.; Xue, A.; Lin, T.; Zhang, G. The uncertainty and its influence of wind generated power on power system transient stability under different penetration. In Proceedings of the 2014 International Conference on Power System Technology, Chengdu, China, 20–22 October 2014; pp. 675–680.
4. Fambri, G.; Diaz-Londono, C.; Mazza, A.; Badami, M.; Sihvonen, T.; Weiss, R. Techno-economic analysis of Power-to-Gas plants in a gas and electricity distribution network system with high renewable energy penetration. *Appl. Energy* **2022**, *312*, 118743. [CrossRef]
5. Wang, J.; Xu, X.; Li, H.; Chen, H. Two-stage robust optimization of thermal-ESS units scheduling under wind uncertainty. *Energy Rep.* **2022**, *8* (Suppl. 5), 1147–1155. [CrossRef]
6. Roald, L.A.; Sundar, K.; Zlotnik, A.; Misra, S.; Andersson, G. An Uncertainty Management Framework for Integrated Gas-Electric Energy Systems. *Proc. IEEE* **2020**, *108*, 1518–1540. [CrossRef]
7. Clegg, S.; Mancarella, P. Integrated Modeling and Assessment of the Operational Impact of Power-to-Gas (P2G) on Electrical and Gas Transmission Networks. *IEEE Trans. Sustain. Energy* **2015**, *6*, 1234–1244. [CrossRef]
8. Zlotnik, A.; Roald, L.; Backhaus, S.; Chertkov, M.; Andersson, G. Coordinated Scheduling for Interdependent Electric Power and Natural Gas Infrastructures. *IEEE Trans. Power Syst.* **2017**, *32*, 600–610. [CrossRef]
9. Bai, L.; Li, F.; Cui, H.; Jiang, T.; Sun, H.; Zhu, J. Interval optimization based operating strategy for gas-electricity integrated energy systems considering demand response and wind uncertainty. *Appl. Energy* **2016**, *167*, 270–279. [CrossRef]
10. Alvarez, G.E. Stochastic optimization considering the uncertainties in the electricity demand, natural gas infrastructures, photovoltaic units, and wind generation. *Comput. Chem. Eng.* **2022**, *160*, 107712. [CrossRef]
11. Li, G.; Zhang, R.; Jiang, T.; Chen, H.; Bai, L.; Li, X. Security-constrained bi-level economic dispatch model for integrated natural gas and electricity systems considering wind power and power-to-gas process. *Appl. Energy* **2017**, *194*, 696–704. [CrossRef]
12. Xue, Y.; Lei, X.; Xue, F. A review on impacts of wind power uncertainties on power systems. *Proc. CSEE* **2014**, *34*, 5029–5040.
13. Qiu, F.; Wang, J. Chance-Constrained Transmission Switching with Guaranteed Wind Power Utilization. *IEEE Trans. Power Syst.* **2015**, *30*, 1270–1278. [CrossRef]
14. Duan, J.; Yang, Y.; Liu, F. Distributed optimization of integrated electricity-natural gas distribution networks considering wind power uncertainties. *Int. J. Electr. Power Energy Syst.* **2022**, *135*, 107460. [CrossRef]
15. Liang, Z.; Chen, H.; Chen, S.; Wang, Y.; Zhang, C.; Kang, C. Robust Transmission Expansion Planning Based on Adaptive Uncertainty Set Optimization Under High-Penetration Wind Power Generation. *IEEE Trans. Power Syst.* **2021**, *36*, 2798–2814. [CrossRef]
16. Almasabi, S.; Sulaeman, S.; Nguyen, N.; Mitra, J. Cost benefit analysis for wind power penetration. In Proceedings of the 2017 North American Power Symposium (NAPS), Morgantown, WV, USA, 17–19 September 2017; pp. 1–6.
17. Shahidehpour, M.; Fu, Y.; Wiedman, T. Impact of Natural Gas Infrastructure on Electric Power Systems. *Proc. IEEE* **2005**, *93*, 1042–1056. [CrossRef]
18. Zeng, Q.; Zhang, B.; Fang, J.; Chen, Z. Coordinated Operation of the Electricity and Natural Gas Systems with Bi-directional Energy Conversion. *Energy Procedia* **2017**, *105*, 492–497. [CrossRef]
19. Zhang, Z.; Zhang, Y.; Huang, Q.; Lee, W. Market-oriented optimal dispatching strategy for a wind farm with a multiple stage hybrid energy storage system. *CSEE J. Power Energy Syst.* **2018**, *4*, 417–424. [CrossRef]
20. Liu, J.; Bao, H. Research on interest coordination model of wind power supply chain with energy storage participation. *J. Energy Storage* **2022**, *49*, 104107. [CrossRef]
21. Dadashi, M.; Zare, K.; Seyedi, H.; Shafie-khah, M. Coordination of wind power producers with an energy storage system for the optimal participation in wholesale electricity markets. *Int. J. Electr. Power Energy Syst.* **2022**, *136*, 107672. [CrossRef]
22. Luo, W.; Feng, S.; Ge, W.; Wang, Z. Research on the control strategy of large-scale wind power energy storage system. In Proceedings of the IEEE PES Innovative Smart Grid Technologies, Tianjin, China, 21–24 May 2012; pp. 1–4.
23. Li, Y.; Wang, J.; Han, Y.; Zhao, Q.; Fang, X.; Cao, Z. Robust and opportunistic scheduling of district integrated natural gas and power system with high wind power penetration considering demand flexibility and compressed air energy storage. *J. Clean. Prod.* **2020**, *256*, 120456. [CrossRef]
24. De Boer, H.S.; Grond, L.; Moll, H.; Benders, R. The application of power-to-gas, pumped hydro storage and compressed air energy storage in an electricity system at different wind power penetration levels. *Energy* **2014**, *72*, 360–370. [CrossRef]

25. Ye, S.; Liu, T.; Zhang, Q.; He, C.; Nan, L. Chance-constrained Optimal Scheduling of Integrated Gas-electric System. In Proceedings of the 2021 Power System and Green Energy Conference (PSGEC), Shanghai, China, 20–22 August 2021; pp. 531–536.
26. Wang, C.; Wang, Z.; Wang, J.; Hou, Y. Chance-constrained maintenance scheduling for interdependent power and natural gas grids considering wind power uncertainty. *IET Gener. Transm. Distrib.* **2019**, *13*, 686–694. [CrossRef]
27. He, C.; Wu, L.; Liu, T.; Wei, W.; Wang, C. Co-optimization scheduling of interdependent power and gas systems with electricity and gas uncertainties. *Energy* **2018**, *159*, 1003–1015. [CrossRef]